

JAERI-Research  
99-010



JP9950115



NEUTRONIC STUDIES OF BARE TARGETS FOR JAERI 5 MW  
PULSED SPALLATION NEUTRON SOURCE

February 1999

Makoto TESHIGAWARA, Noboru WATANABE,  
Hiroschi TAKADA, Hiroschi NAKASHIMA, Tadashi NAGAO,  
Yukio OYAMA and Kazuaki KOSAKO\*

日本原子力研究所  
Japan Atomic Energy Research Institute

本レポートは、日本原子力研究所が不定期に公刊している研究報告書です。  
入手の問い合わせは、日本原子力研究所研究情報部研究情報課（〒319-1195 茨城県那珂郡東海村）あて、お申し越し下さい。なお、このほかに財団法人原子力弘済会資料センター（〒319-1195 茨城県那珂郡東海村日本原子力研究所内）で複写による実費領布を行っております。

This report is issued irregularly.  
Inquiries about availability of the reports should be addressed to Research Information Division, Department of Intellectual Resources, Japan Atomic Energy Research Institute, Tokai-mura, Naka-gun, Ibaraki-ken 319-1195, Japan.

© Japan Atomic Energy Research Institute, 1999

編集兼発行 日本原子力研究所

Neutronic Studies of Bare Targets for JAERI 5 MW Pulsed Spallation  
Neutron Source

Makoto TESHIGAWARA\*, Noboru WATANABE\*\*, Hiroshi TAKADA,  
Hiroshi NAKASHIMA, Tadashi NAGAO, Yukio OYAMA and  
Kazuaki KOSAKO\*

Center for Neutron Science  
Tokai Research Establishment  
Japan Atomic Energy Research Institute  
Tokai-mura, Naka-gun, Ibaraki-ken

(Received January 26, 1999)

We report the results for neutronic calculations (effect of target shape and material) on various bare targets to be implemented in a next generation pulsed spallation neutron source in Japan Atomic Energy Research Institute. A flat target gives a much higher leakage neutron intensity than a cylindrical one and a mercury target gives a higher leakage neutron intensity than a leadbismuth eutectic target. The effect of the target shape on the leakage neutron intensity is discussed to determine the optimal shape and size, although rigorous calculations on whole systems of target-moderator-reflector is indispensable to assess accurate neutronic performance. The nuclear heating in a light water sample located at 2 cm from the target surface was also estimated as a function of target depth, in order to obtain a rough information on energy deposition in cryogenic moderators.

Keywords: Intense Spallation Neutron Source, Bare Target, Optimal Target Shape, Neutronic Performance, Leakage Neutrons, Moderator, Nuclear Heating,

---

\* Post-Doctoral Fellow

\*\* Scientific Consultant

\* Sumitomo Atomic Power Industries Ltd.

JAERI 5 MW 短パルス核破砕中性子源開発のための裸のターゲット  
より得られる中性子のニュートロニクス研究

日本原子力研究所東海研究所中性子科学研究センター  
勅使河原 誠\*・渡辺 昇\*\*・高田 弘・中島 宏  
永尾 忠司・大山 幸夫・小迫 和明\*

(1999年1月26日受理)

原研中性子科学研究計画で次世代短パルス核破砕中性子源の建設を目指しており、その第一歩として裸のターゲットから漏洩する中性子に関するニュートロニクス計算(ターゲット形状やターゲット材料等による)を行った。円筒形のターゲットに比べ扁平ターゲットは遥かに高い漏洩中性子束をモデレータに供給することが出来ること、水銀ターゲットは鉛・ビスマス共融体ターゲットに比べ高い漏洩中性子強度を与えること等が明らかとなった。また、どのようなターゲットの形状が高い中性子強度を与えるのか等に関して重要な知見を得た。しかしながら、正確に中性子性能を評価するためにターゲット・モデレータ・反射体系を含めた計算は不可避である。また、冷モデレータにおける核発熱の情報を得るために、ターゲットに近接(ターゲット表面から2 cm)して置かれた軽水の核発熱分布を求めた。

---

東海研究所:〒319-1195 茨城県那珂郡東海村白方白根2-4

\* 博士研究員

\*\* 特別研究員

\* (株)住友原子力工業

## Contents

1. Introduction .....	1
2. Calculational Model .....	1
3. Calculations .....	2
4. Calculated Results .....	2
4.1 Cylindrical Targets .....	2
4.2 Rectangular (flat) Targets .....	4
4.3 Energy Deposition in water sample at 2cm from target surface .....	4
5. Conclusions .....	5
References .....	5

## 目 次

1. 概 要 .....	1
2. 計算モデル .....	1
3. 計 算 法 .....	2
4. 計算結果 .....	2
4.1 円筒形ターゲット .....	2
4.2 扁平ターゲット .....	4
4.3 ターゲットより 2 cm 離れた水の核発熱 .....	4
5. 結 論 .....	5
参考文献 .....	5

This is a blank page.

## 1. Introduction

We started extensive studies on concept of target-moderator-reflector system for the JAERI 5 MW pulsed spallation neutron source<sup>1)</sup>. In this paper main purpose is to gain the information of bare target neutronics, which is important for coupling and optimization of target-moderator-reflector system. As the first step, we performed neutronic calculations for various targets in order to provide primary information for further studies on target-moderator-reflector systems. In the present study we focused on liquid heavy metal targets of lead-bismuth (Pb-Bi) and mercury (Hg) as references. This report describes the results of the studies, especially on the axial distribution of leakage neutrons and protons from bare targets of different materials and shapes. The axial distribution of energy deposition in a 1 cm<sup>3</sup> water (H<sub>2</sub>O) sample located at 2 cm from the side surface target was calculated to estimate approximate values for the energy deposition in cryogenic moderators.

## 2. Calculational model

Table 1 summarizes the main parameters of incident proton beam, target shapes and materials considered in the present study. The calculational models for different targets (in shape/size and material) with beam profiles are schematically illustrated in Fig. 1. The lateral sizes or a diameter of the target are larger than those of the proton beam profile. The radial or lateral thickness of the target region out of the proton beam is one of the most important parameters because the neutronic performance and the nuclear heating in cryogenic moderators strongly depend on this thickness; thinner the better from the total neutron yield point of view, while thicker the better to reduce the nuclear heating in cryogenic moderators.

In the present study we assumed that this thickness is 1.5 cm for cylindrical targets, while for rectangular targets 1.5 cm to the vertical direction (towards the moderators) and 2.0 cm to the horizontal direction. The required thickness should be finally determined from technical points of view, e.g. the spatial stability of the proton beam on the target and the nuclear heating of cryogenic moderators at the minimum cost in neutron intensity. The model targets have a sort of dome window with a hemisphere shape as illustrated in Fig. 1 and the length of the targets was fixed at 40 cm in all cases. We assumed that the maximum acceptable current density of the proton beam is 48  $\mu\text{A}/\text{cm}^2$  judging from the maximum acceptable thermal stress in the incident window; this value is also accepted recently at other intense spallation neutron source projects. We also studied for a lower current density of 24  $\mu\text{A}/\text{cm}^2$  by keeping the total proton beam current at the same value. We assumed uniform (flat) profiles of the proton beam in all cases, since the beam size can be minimized with an uniform profile compared with parabolic or Gaussian cases. A smaller beam size, accordingly a smaller target cross section will provide a higher leakage neutron intensity. On the other hand, a smaller beam size, accordingly a smaller target

will result in a higher mechanical stress due to higher center temperature. The effect of an uniform beam profile on the mechanical stress of the Hg target container, especially in the incident window will be discussed elsewhere<sup>2)</sup>.

### 3. Calculations

We performed some neutronic calculations using both code systems NMTC/JAERI<sup>3,4)</sup> which treats the high energy hadron transport (above 20 MeV) and MCNP-4A<sup>5)</sup> with cross section set (FSXLIB-JEFF, FSXLIB-JFNS and THERXS) which handles the neutron transport below 20 MeV. The latter is a Monte Carlo code which has most widely been used at various neutronic calculation. The total number of the energy group mesh was 81 as shown in Fig. 2. In the case of a mercury (Hg) target, cross sections recently evaluated at JAERI were used<sup>6)</sup>. The total number of protons incident upon the target to produce neutrons was about  $8 \times 10^5$  in each Monte Carlo simulation in NMTC/JAERI. The number of protons was determined so that the maximum statistical error of neutron intensity per unit energy bin was less than 1%.

### 4. Calculated results

#### 4.1 Cylindrical targets

Figure 3 shows the axial distributions of leakage neutrons from the cylindrical Hg target of the diameter of 12.36 cm for both low energy ( $< 20$  MeV) and total energy neutrons. The distributions can be characterized by the peak position, the peak intensity and the width (full width at half maximum, FWHM), and they are followed by an exponential decay (characteristic attenuation length). It can be seen from this figure that the peak appears at about 8-10 cm from the incident surface with a width of about 26 cm and an attenuation length of about 14 cm. Although the peak region is somewhat broader than the case of 800 MeV protons in LANSCE (the Los Alamos Neutron Science Center), which has highest proton energy in existing spallation neutron source facility. It is still too narrow if we want to position two moderators on each side (above or below the target) of the target as described in the succeeding paper<sup>7)</sup>. The region of 8-10 cm from the incident surface is considered to be most effective to supply source neutrons to a moderator. For a reference we also plotted the axial distribution of leakage protons from the target.

The neutron energy spectra (at  $Z = 8-10$  cm depth) from various targets, including some water-cooled solid targets, are compared in Fig. 4, where the intensities are in the absolute unit (flux spectrum). As well known each spectrum composes of, at least, two components, i.e., evaporation/fission ( $< 20$  MeV) and high energy ( $> 20$  MeV) neutrons. The peak positions in the energy spectra from the Hg target and the solid targets of W and Ta appear around at the same



energy, while the Pb-Bi eutectic target exhibits a harder spectrum with a lower peak intensity. Two solid targets with cooling water (homogenous mixture of 10 % H<sub>2</sub>O) exhibit much softer spectrum. The softening of energy spectrum itself does not affect on a slow neutron intensity from a moderator when we install a moderator adjacent to the target. Because the total neutronic performance can not be discussed only from the above results. Hence full calculations of a target-moderator-reflector system is indispensable to optimize target shape and material, as will be discussed in the succeeding paper<sup>7)</sup>.

Figures 5 and 6 show the spectral intensities at four regions of different axial positions along the target axis (see the insets) for cylindrical Hg and Pb-Bi targets of a diameter of 12.36 cm, respectively. The spectral intensity (at Z = 8-10 cm from the both targets) gives the highest intensity of low energy neutron region (< 20 MeV). At farther distances from the incident surface the intensity of high energy neutrons is more pronounced due to a forward angular distribution of high-energy neutrons.

Figure 7 compares the spectral intensities from the Hg and the Pb-Bi targets of different target diameters. It can be clearly seen that at higher energies above the peak position the intensities are almost the same (independent of target size and material), while at lower energies, the Hg targets provide a higher intensities. The difference in target size (diameter) does not bring about an appreciable difference in the log-log plots. On the other hand, there is a considerable material dependence at the low energy region.

We also studied on leakage protons from the targets. Figure 8 compares the spectral intensities of leakage neutrons and protons from the cylindrical Hg target of 12.36 cm in diameter at Z = 8-10 cm from the incident surfaces. The ratio of proton in total leakage particle is small, about 0.4 % however it causes nuclear heating out of the target.

In Fig. 9 we compare the axial distributions of leakage neutrons and protons from various targets. The Hg target of a smaller diameter gives highest neutron intensity than those of the other targets. The intensities from the Hg targets are higher than those from the Pb-Bi targets. The axial distributions of leakage protons integrated over an entire energy range are also plotted in this figure.

Figures 10 and 11 show the spectral intensities of leakage protons from different regions of the targets as indicated in the insets. At farther distances from the incident surface, the spectra at higher-energies are much enhanced. These data provide information on the optimal position of a cryogenic moderator from a point of nuclear heating.

Figure 12 shows the spectral intensities of leakage protons from the various cylindrical targets. Pb-Bi targets give slightly higher proton intensities than the Hg targets, while the smaller targets (smaller diameter) give much higher proton intensities than the larger ones.

## 4.2 Rectangular (flat) targets

Figure 13 shows the neutron spectral intensities from a rectangular (flat) Hg target of  $9.88^H \times 14^W$  cm<sup>2</sup> at four different axial positions along the target axis as indicated in the inset (at the “center” region as indicated). The energy spectrum are almost the same as those of cylindrical targets, but with a higher intensities because of luminosity region of flatter target shape.

Figure 14 shows the spectral intensities of leakage neutrons at  $Z = 8-10$  cm and at three different regions on the rectangular Hg target of  $9.88^H \times 14.0^W$  cm<sup>2</sup>. Each region, “center”, “middle”, and “outer”, corresponds to one third of the area on the target as depicted in the inset. The intensities from “center” and “middle” are almost comparable and those from “outer” are about 60 % of the others, suggesting that the higher intensity region is fairly large over the lateral length.

We also studied the dependencies of material and the size of the rectangular targets on the spectral intensities at  $Z = 8-10$  cm. The results are shown in Fig.15. The spectra from the targets of different shapes ( $9.88^H \times 14^W$  cm<sup>2</sup> and  $6.44^H \times 24^W$  cm<sup>2</sup>) are almost the same. A full calculation for a complete target-moderator-reflector system, however is indispensable in the next stage to judge which shape is the optimal.

Figure 16 shows the axial distributions of neutrons and protons from the rectangular Hg target ( $9.88^H \times 14^W$  cm<sup>2</sup>) in three different regions “center”, “middle” and “outer”. Again the intensity difference between “center” and “middle” is small.

Figure 17 shows similar results from the thinner Hg target ( $6.44^H \times 24^W$  cm<sup>2</sup>). From the comparison of both results (Figs. 16 and 17), the peak intensities are almost comparable ( the thicker target provides slightly higher intensity). On the other hand, thinner target gives slightly higher leakage proton intensities than thicker one.

Figure 18 compares the axial distributions of leakage neutrons from all targets studied of different materials and shapes. The results for the cylindrical targets are also plotted for comparison. A Hg target ( $9.88^H \times 14^W$  cm<sup>2</sup>) in center region provides a higher leakage neutron intensities than other targets as far as bare target neutronics are concerned.

## 4.3 Energy Deposition in water sample at 2cm from target surface

In order to estimate approximate values for the nuclear heating of cryogenic moderator, we surveyed the energy deposition using a small H<sub>2</sub>O sample at a distance of 2 cm from the target as a function of axial length  $Z$  as shown in Fig. 19. The axial dependence is more or less similar to that of the leakage neutron intensity. There is no appreciable difference between the two different flatness. The material dependence of the targets on the energy deposition is also small. However at larger distances the Pb-Bi targets give higher values due to a smaller atomic number density compared with that of Hg.

## 5 Conclusions

From the present studies we arrived at the following conclusions :

- (1) As far as bare target neutronics are concerned, a Hg target gives a higher leakage neutron intensity by 20-25 % than a Pb-Bi target (Fig. 18).
- (2) A flat target provide a higher leakage neutron intensity by 30-35 % than a cylindrical target (Fig. 18).
- (3) The effect of the target height on leakage neutron intensity in rectangular targets is rather small, i.e., a rectangular target of the larger height ( $9.88^H \times 14^W$  cm<sup>2</sup>) provides a slightly higher intensity only by 4 % at the peak in the “center” but more in the “middle” and “outer” (Figs. 16 and 17).
- (4) The results on the energy deposition in the 1 cm<sup>3</sup> H<sub>2</sub>O sample show the maximum nuclear heating in the cryogenic moderator is about 23-25 W/cm<sup>3</sup> in H<sub>2</sub>O equivalence, suggesting that a great deal of efforts must be devoted to the cryogenic engineering in order to handle such a higher power.
- (5) The conclusions (2) and (3) suggest that a flat target will provide much higher slow neutron intensities than a cylindrical one, not only due to a higher peak intensity but also to a larger area of highest luminosity region.

However in order to judge which rectangular target (a larger or smaller height) gives a higher slow neutron intensity from a moderator and to determine the optimal dimensions, full calculations on target-moderator-reflector systems are indispensable.

## References

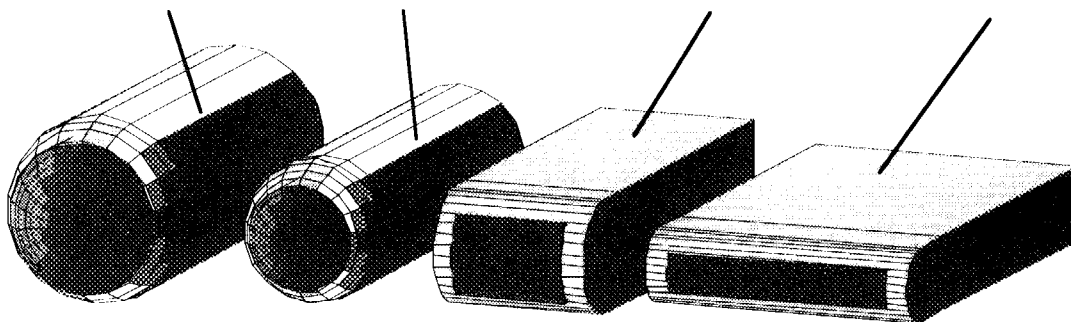
- 1) N. Watanabe, M. Teshigawara, K. Aizawa, J. Suzuki and Y. Oyama : “A target-moderator-reflector concept of the JAERI 5 MW pulsed spallation neutron source”, JAERI Tech 98-011
- 2) S. Ishikura, et al. : to be published
- 3) Y. Nakahara, T. Tsutsui, “NMTC/JAERI, “A Code System for High Energy nuclear Reactions and Nucleon-Meson Transport Code”, JAERI-M 82-198, (1982)
- 4) H. Takada N. Yoshizawa, K. Kosako and K. Ishibashi : “An Upgrade Version of Nuclear Meson Transport Code NMTC / JAERI - 97”, JAERI - Code ( to be published) (1998)
- 5) J. F. Briesmeister (Ed.), “MCNP, A General Monte Carlo N-Particle Transport Code, Version 4A”, LA-12625, (1993)
- 6) K. Shibata, T. Fukahori, S. Chiba and N. Yamamuro, J. Nucl. Sci. Tech. 34 (1997) 1171
- 7) M. Teshigawara, N. Watanabe, H. Takada, H. Nakashima, T. Nagao, Y. Oyama and K. Kosako : “Neutronics study on the JAERI 5 MW Spallation Neutron Source”, to be published in JAERI Research

Table 1 Proton beam profile, target materials and dimensions

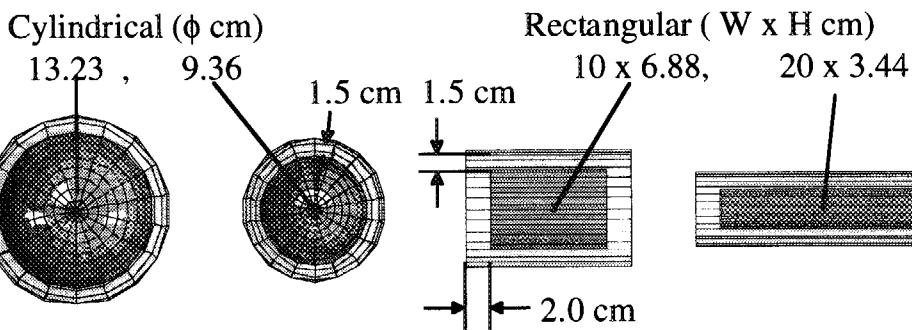
Proton beam			Target			
Energy (GeV)	Profile	Cross section (cm)	Current density ( $\mu\text{A}/\text{cm}^2$ )	Material	Shape	dimension (cm)
1.5	Uniform cylindrical	$\phi$ 13.23	24	Pb-Bi(Eutectic), Hg	Cylindrical	$\phi$ 16.23x40
	Uniform cylindrical	$\phi$ 9.36	48	Pb-Bi(Eutectic), Hg	Cylindrical	$\phi$ 12.36x40
	Uniform rectangular	10x6.88 20x3.44	48	Pb-Bi(Eutectic), Hg	Rectangular	14x9.88x40 24x6.44x40

**Target shapes and dimensions**

Cylindrical ( $\phi$ cm, L cm)		Rectangular ( W x H x L cm <sup>3</sup> )	
(16.23, 40)	(12.36, 40)	(14 x 9.88 x 40)	(24 x 6.44 x 40)



**Proton beam cross section**



**Tally region**

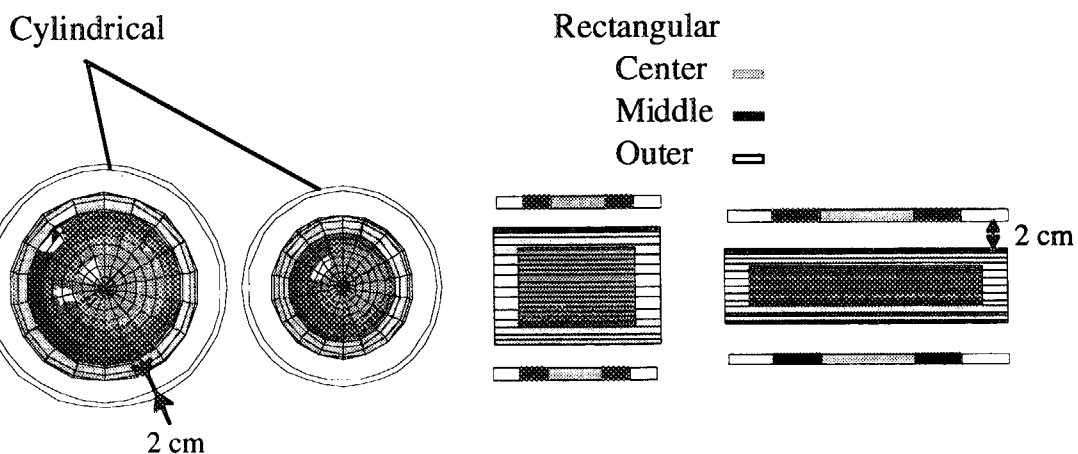


Fig. 1 Geometries of target and proton beam profile (Positions of tally are also indicated)

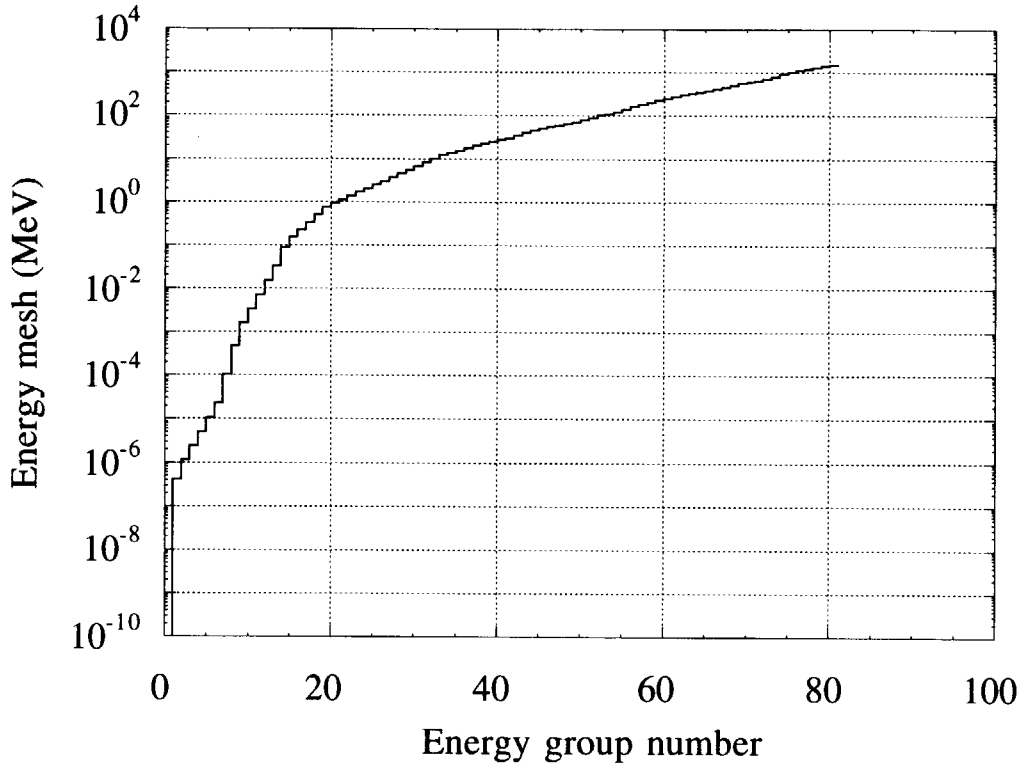


Fig. 2 Relation of energy mesh and energy group number (energy group structure)

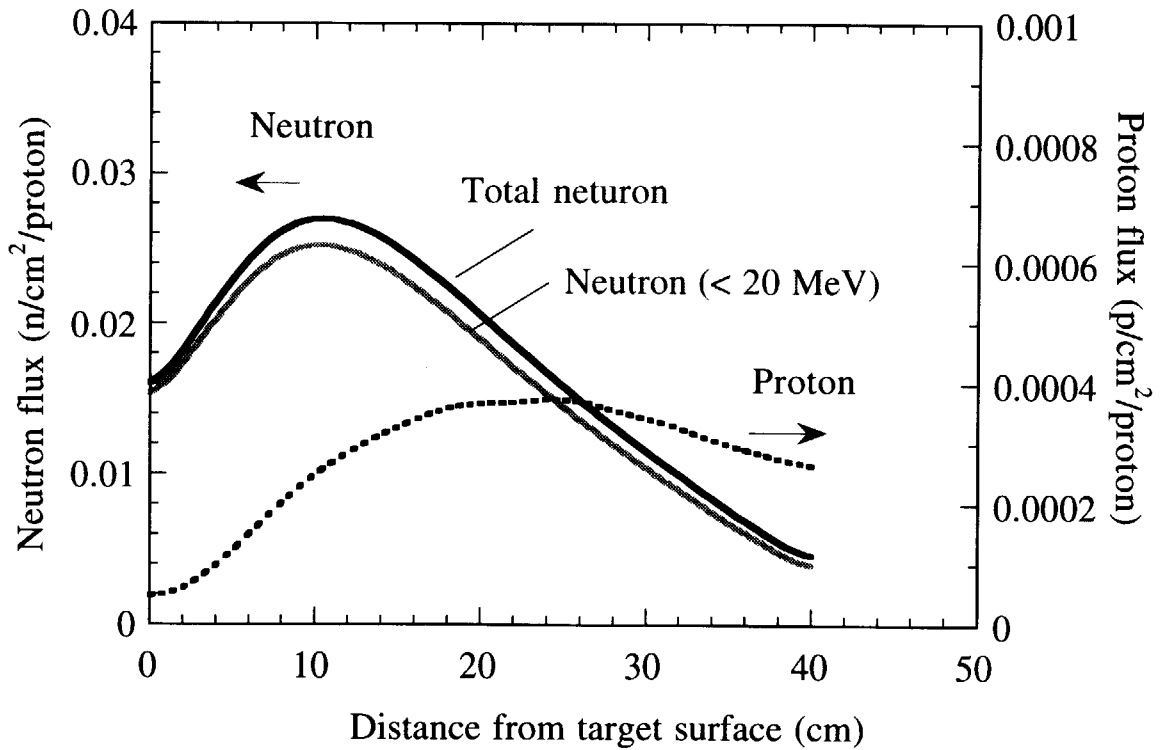


Fig. 3 Axial distribution of neutron and proton intensities leaking from a cylindrical Hg target ( $\phi=12.36\text{cm}$ )

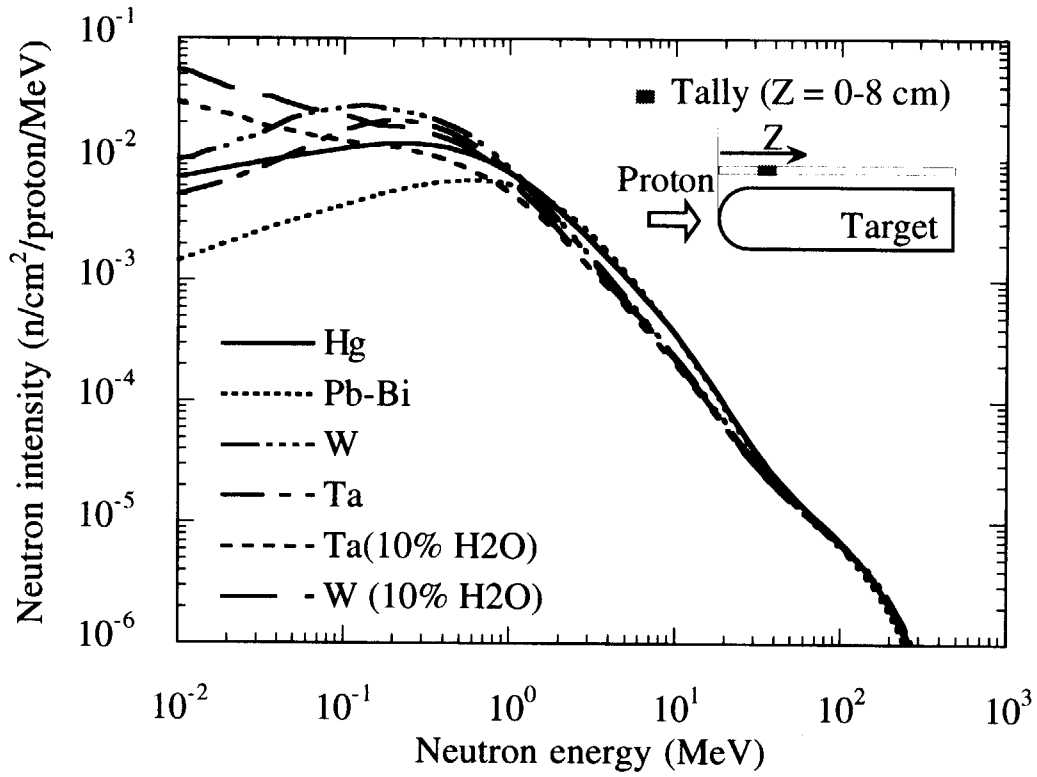


Fig.4 Comparison of leakage neutron from various cylindrical targets ( $\phi=12.36$  cm)

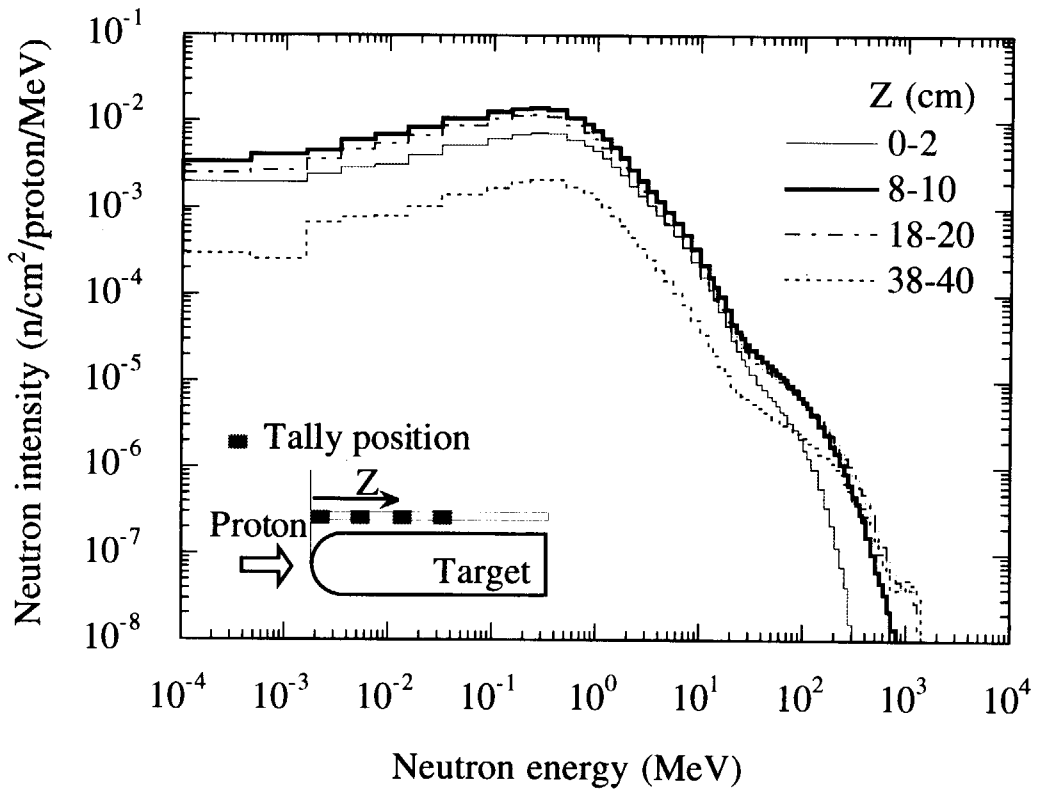


Fig. 5 Position (axial) dependence of spectral intensities of leakage neutrons from a cylindrical Hg target ( $\phi=12.36$  cm)

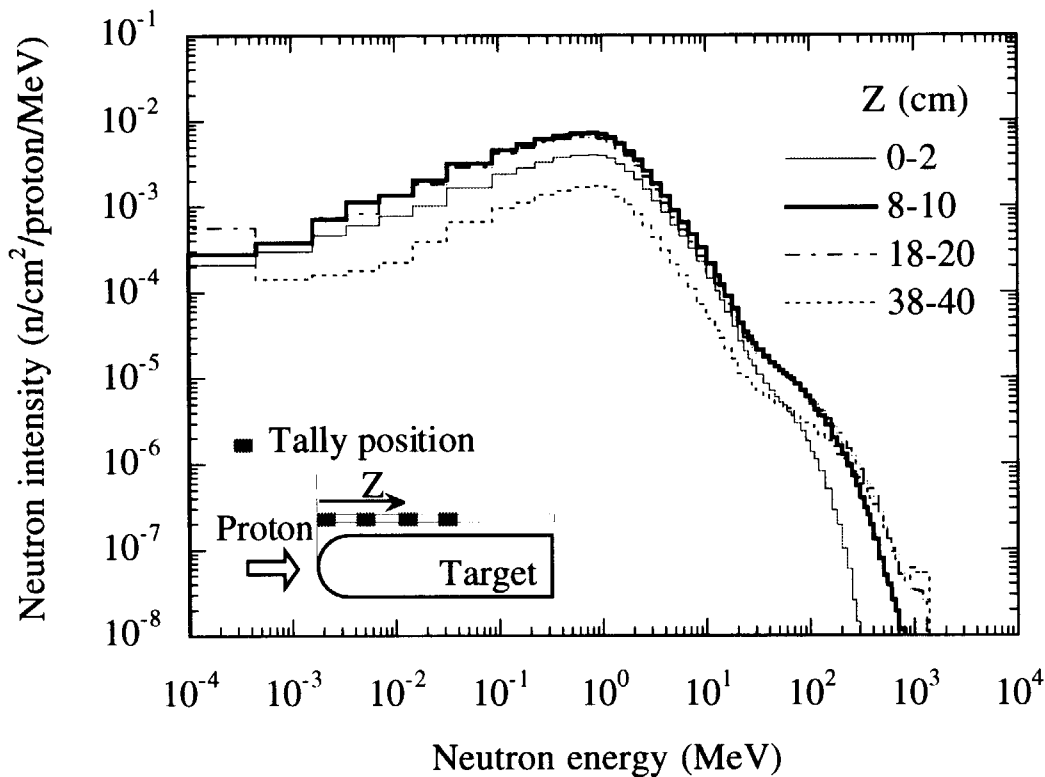


Fig. 6 Position (axial) dependence of spectral intensities of leakage neutrons from a cylindrical Pb-Bi target ( $\phi=12.36$  cm)

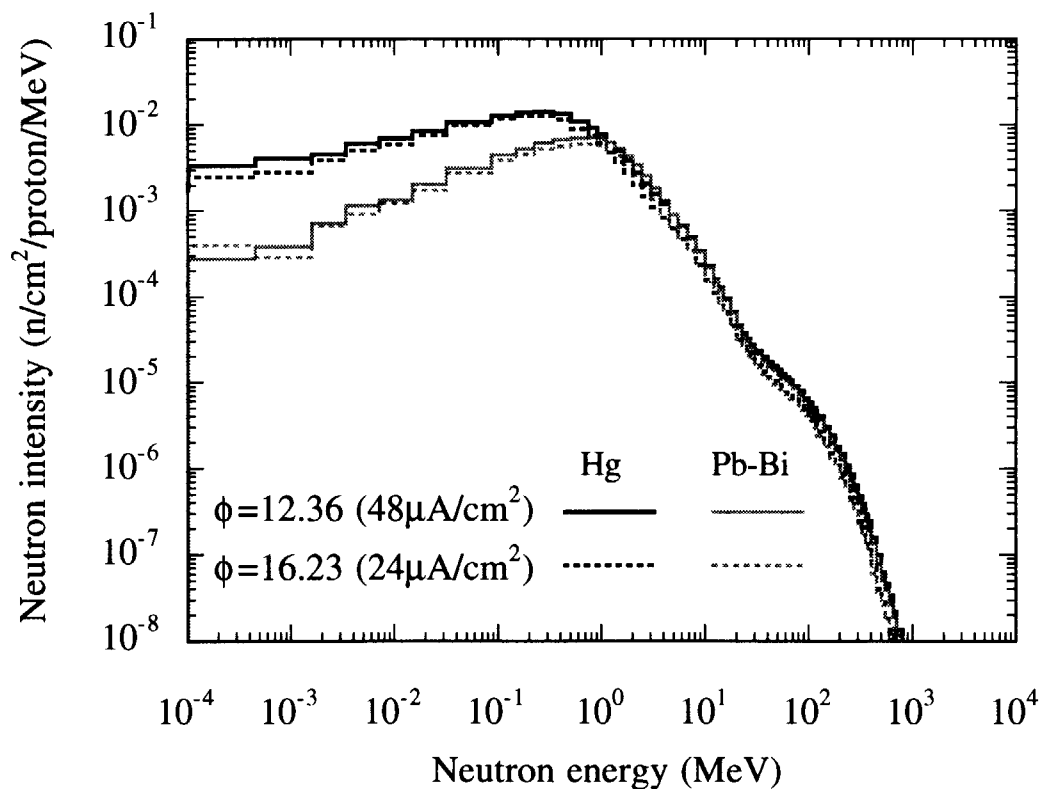


Fig. 7 Target material and diameter dependence of spectral intensities of leakage neutrons from cylindrical targets



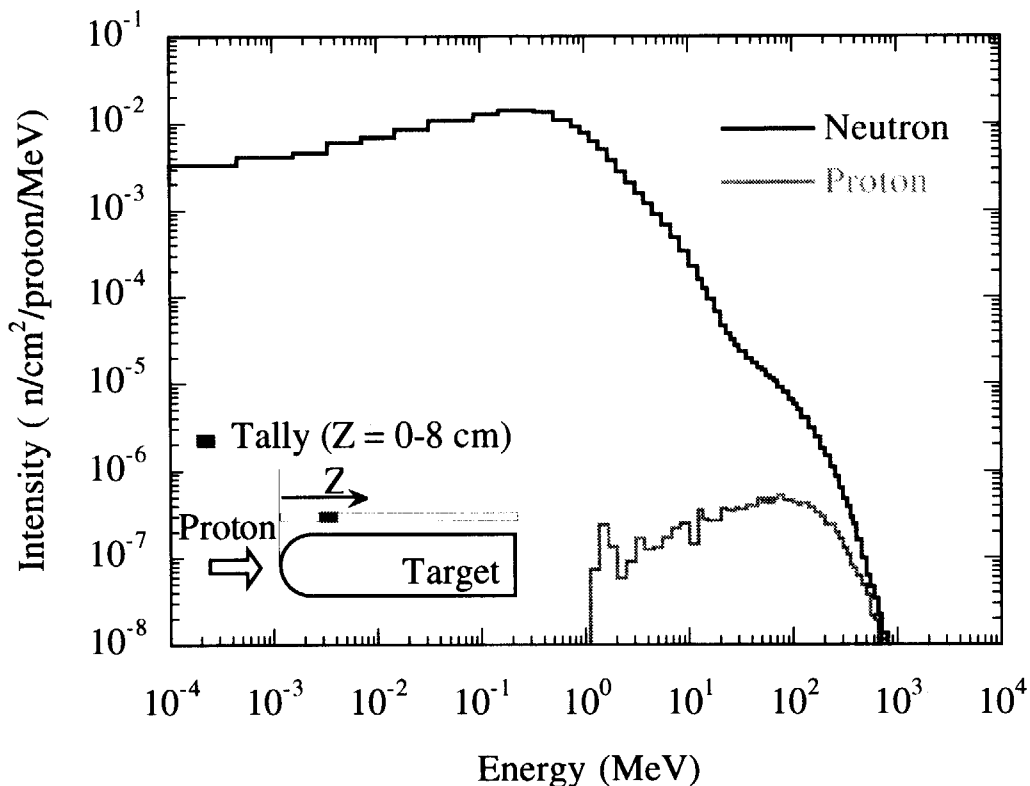


Fig. 8 Spectral intensities of leakage neutron and proton from a cylindrical Hg target ( $\phi=12.36$  cm)

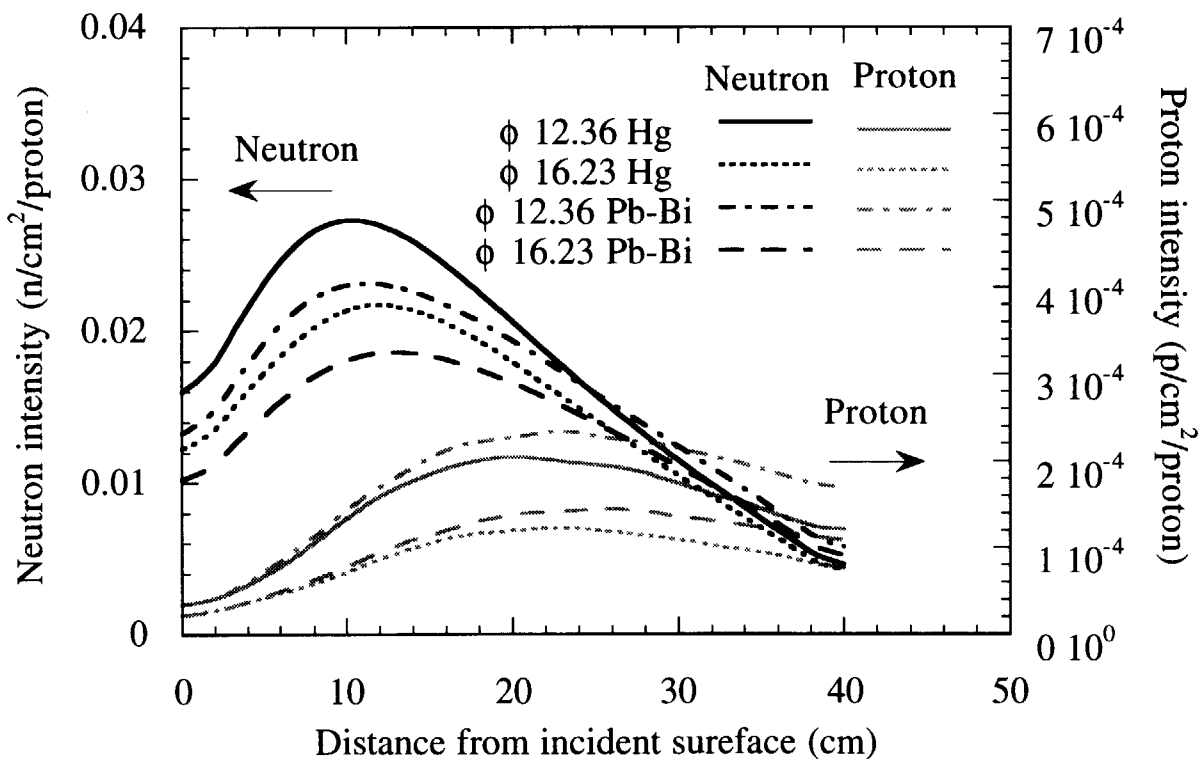


Fig. 9 Spatial (axial) distribution of spectral intensities of leakage neutron and proton from cylindrical targets

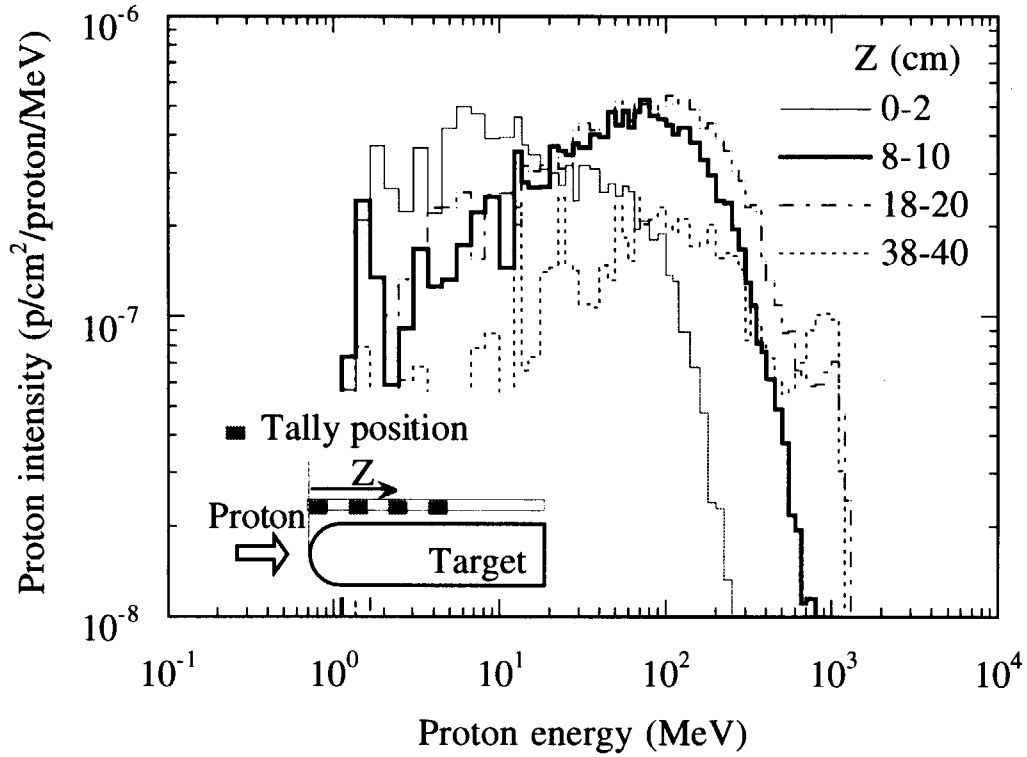


Fig. 10 Position (axial) dependence of spectral intensities of leakage protons from a cylindrical Hg target ( $\phi=12.36$  cm)

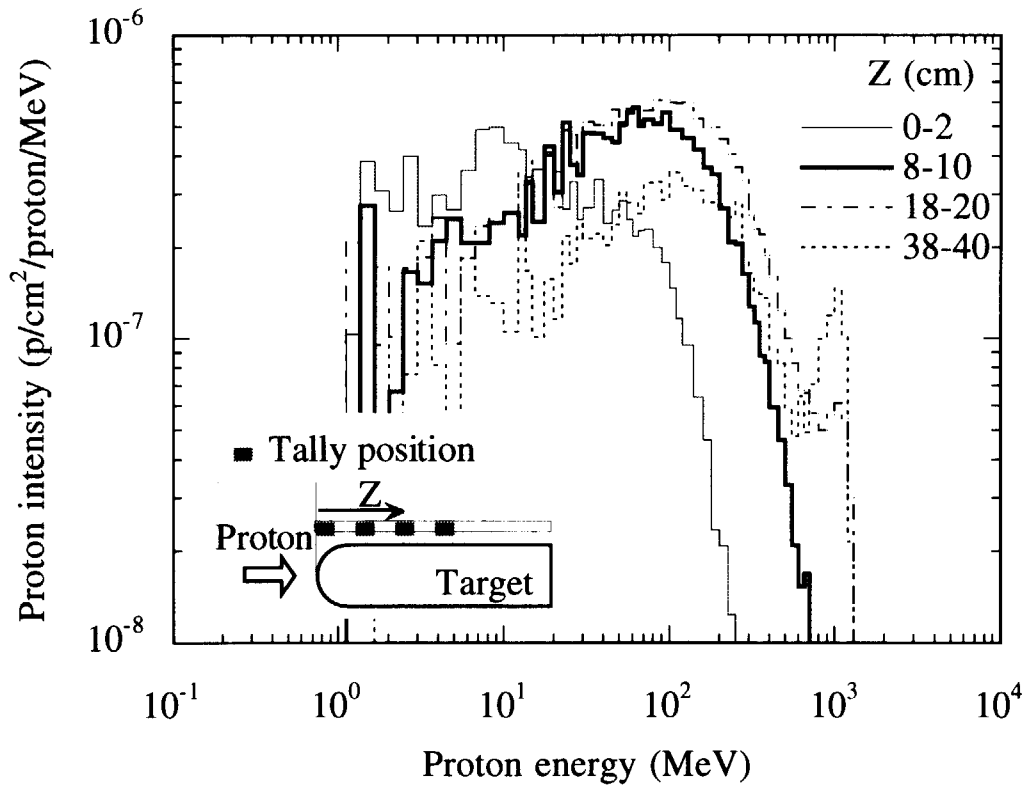


Fig. 11 Position (axial) dependence of spectral intensities of leakage protons from a cylindrical Pb-Bi target ( $\phi=12.36$  cm)

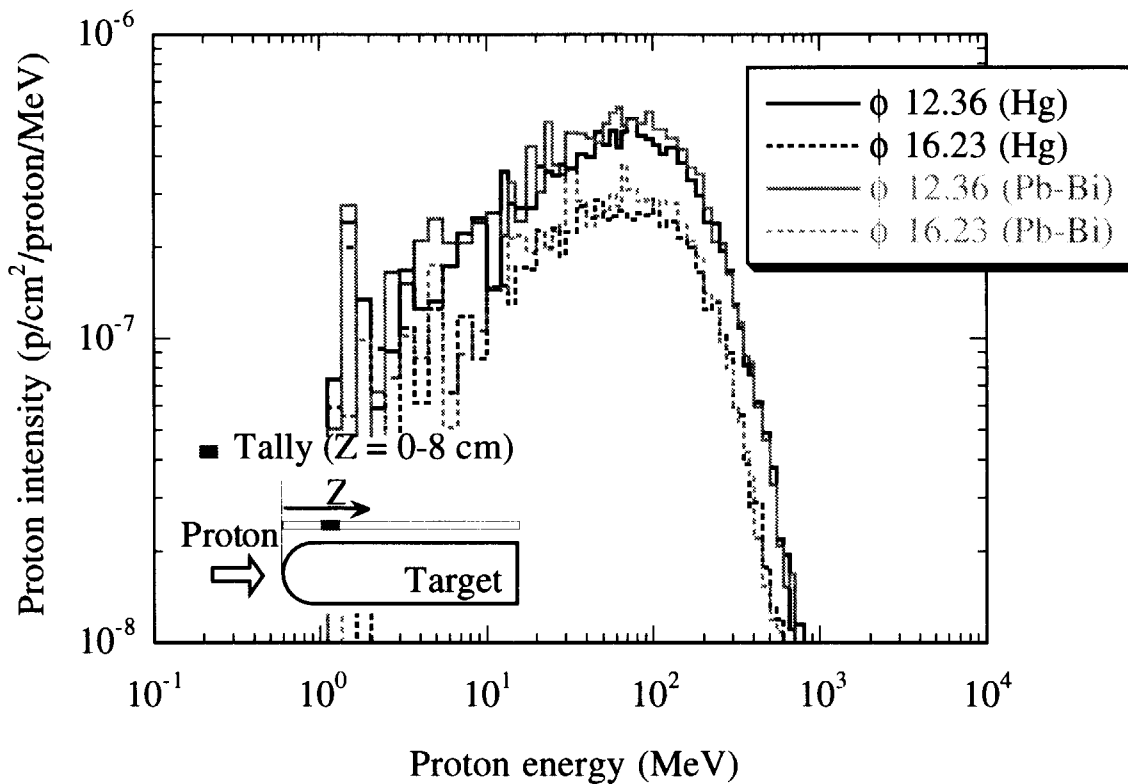


Fig. 12 Target material and diameter dependence of spectral intensities of leakage protons from cylindrical targets

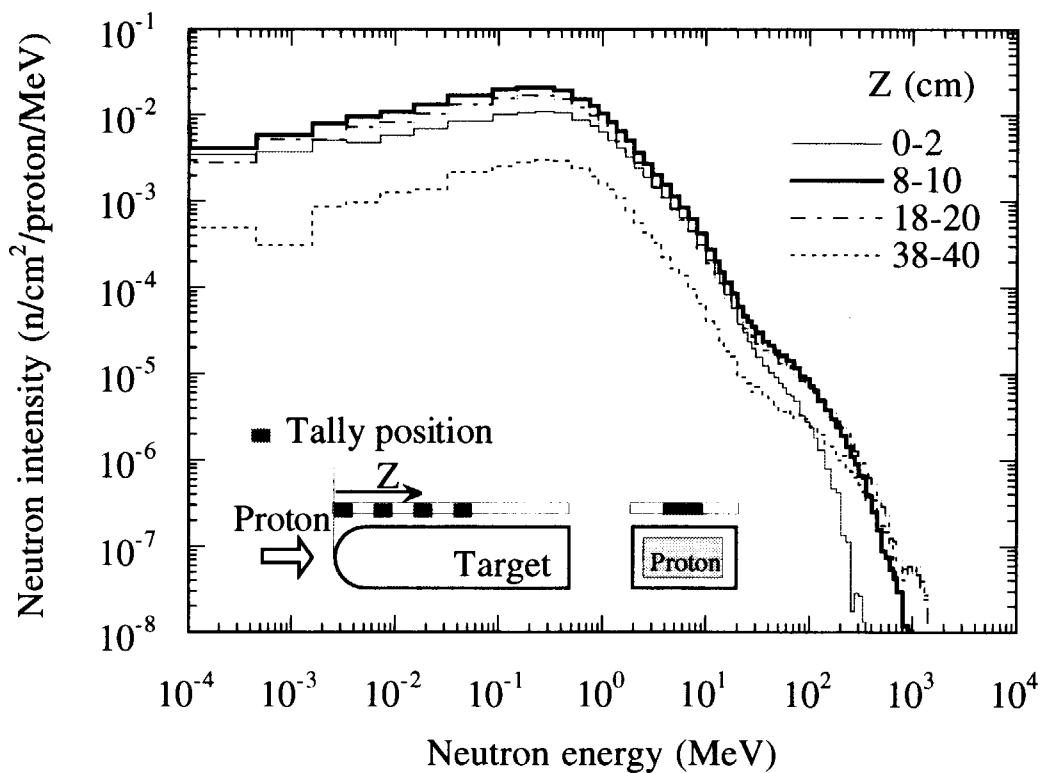


Fig. 13 Position (axial) dependence of spectral intensities of leakage neutrons from a rectangular Hg target ( $14^W \times 9.88^H$  cm<sup>2</sup>)

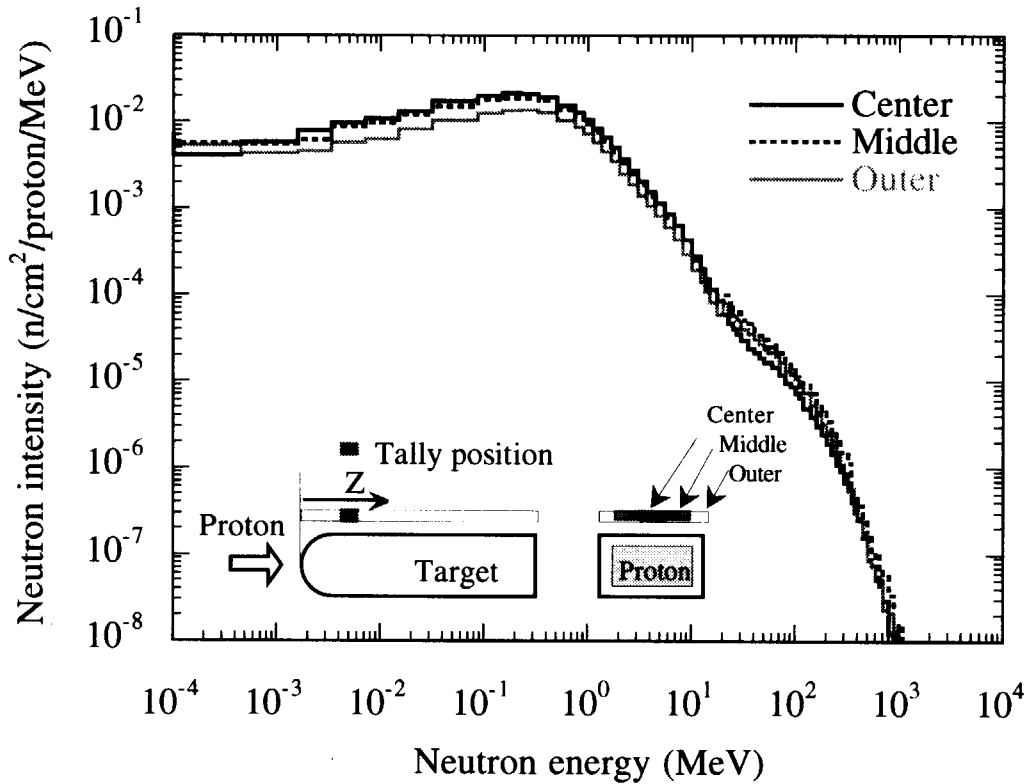


Fig. 14 Positon (lateral) dependence of spectral intensities of leakage neutrons from a rectangular Hg target ( $14^W \times 9.88^H$  cm<sup>2</sup>)

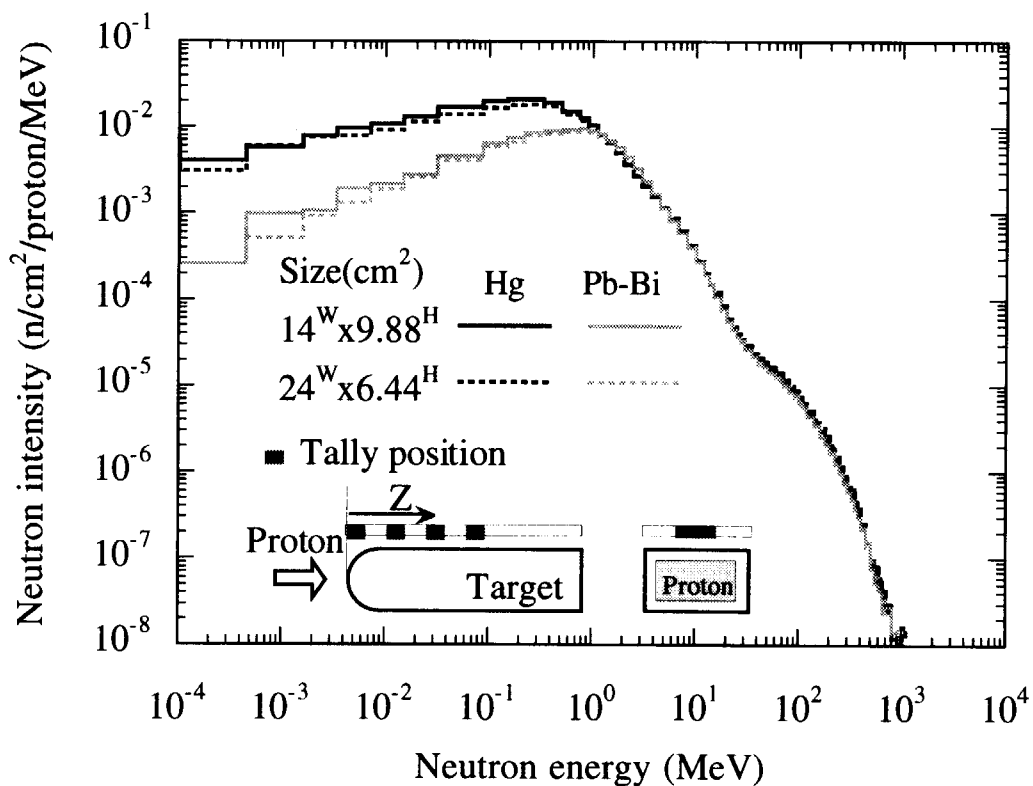


Fig. 15 Target material and shape dependence of spectral intensities of leakage neutrons from rectangular targets

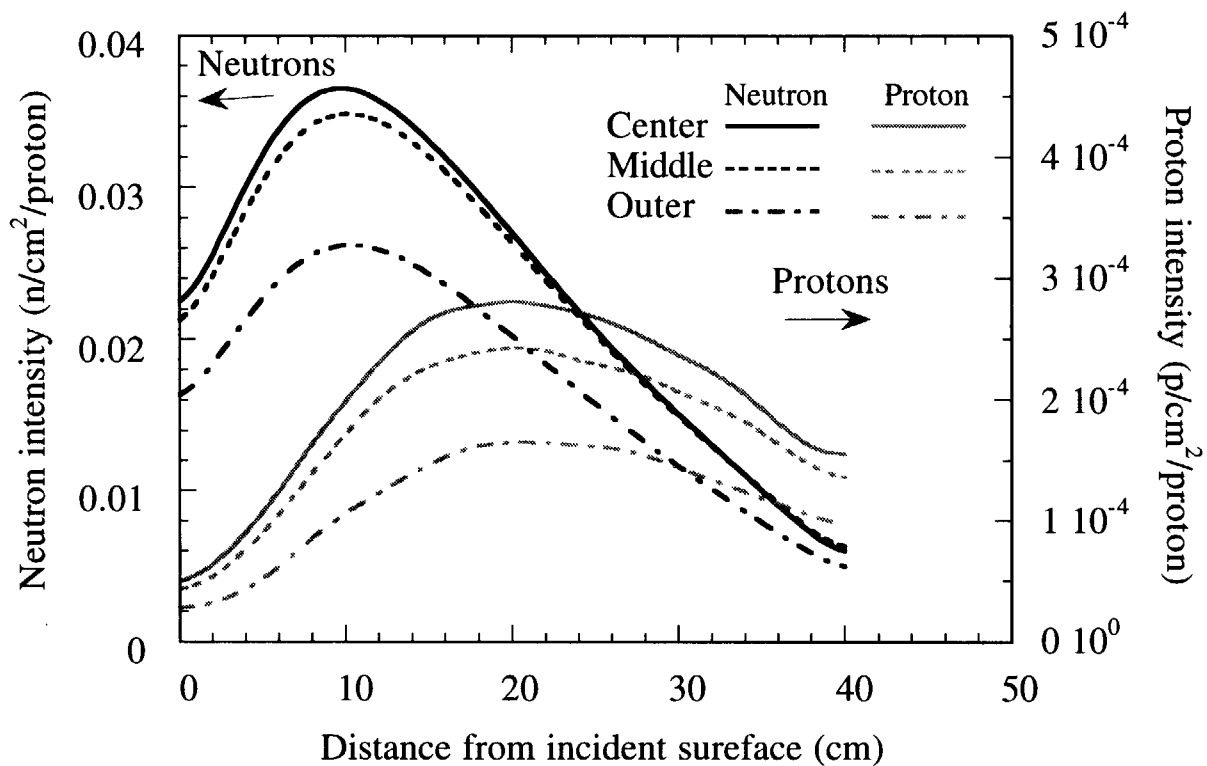


Fig.16 Spatial (axial) distribution of neutron and proton spectral intensities from a rectangular Hg target (14<sup>W</sup>x9.88<sup>H</sup> cm<sup>2</sup>)

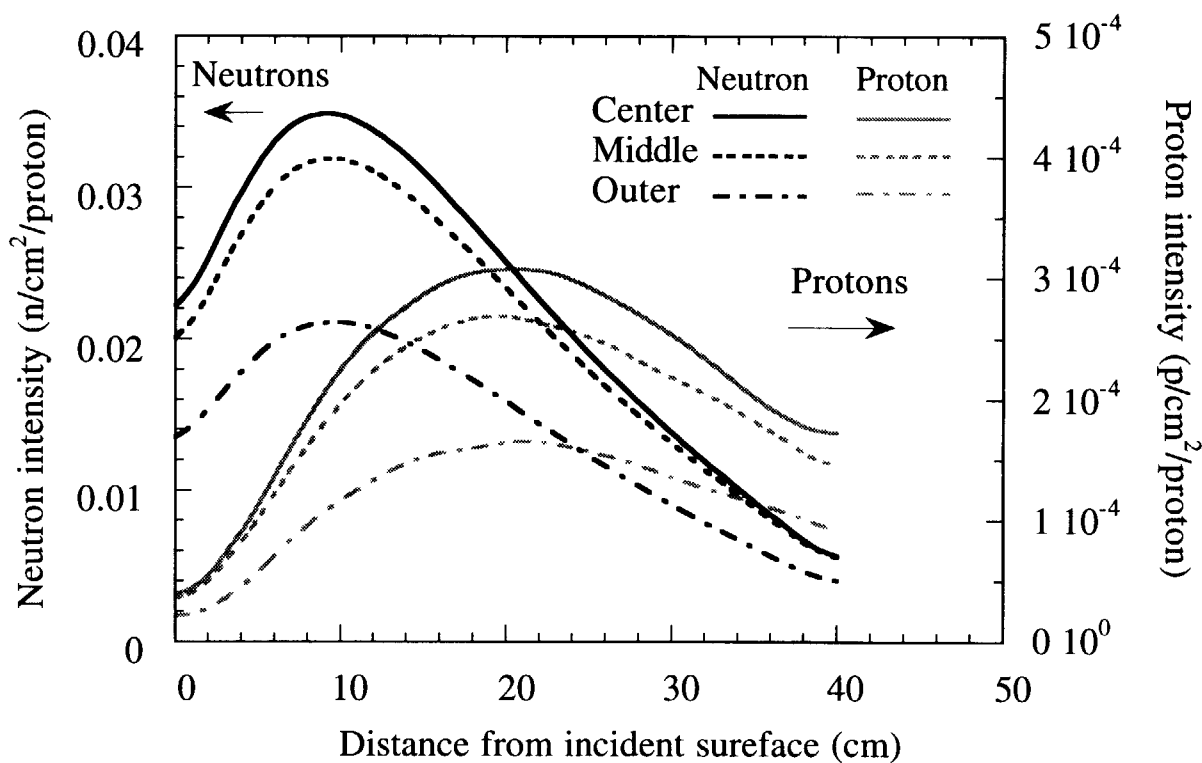


Fig. 17 Spatial (axial) distribution of neutron and proton spectral intensities from a rectangular Hg target (24<sup>W</sup>x6.44<sup>H</sup> cm<sup>2</sup>)

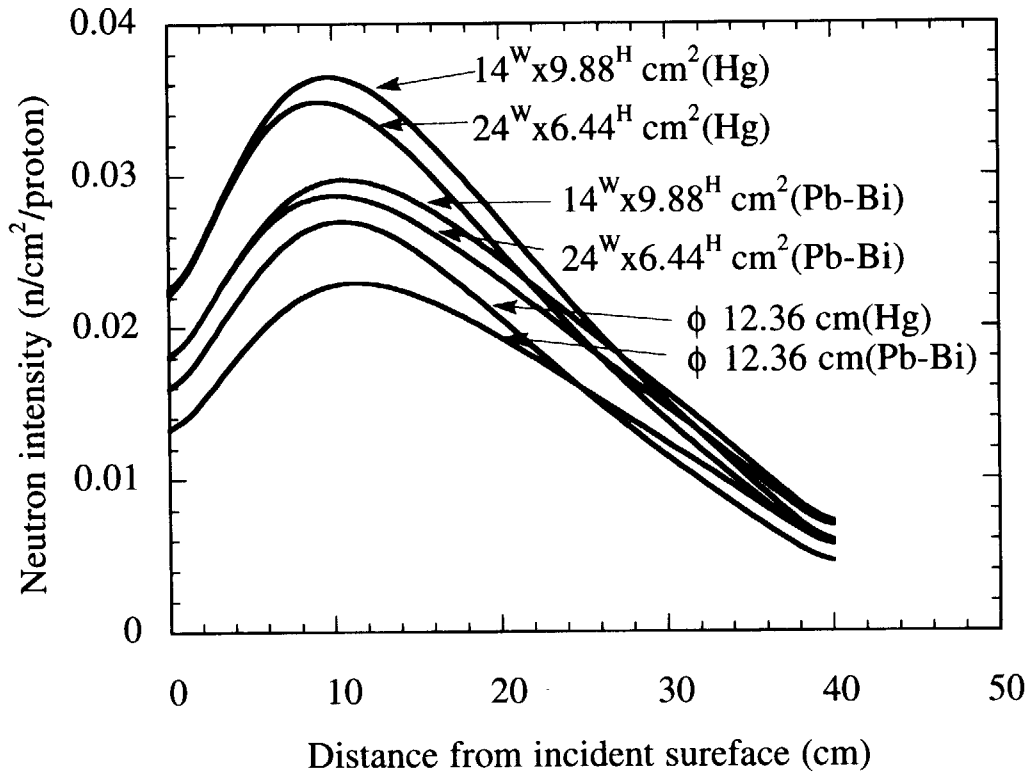


Fig. 18 Spatial (axial) distribution of neutron and proton spectral intensities from various targets. For rectangular targets intensities at center region are only plotted

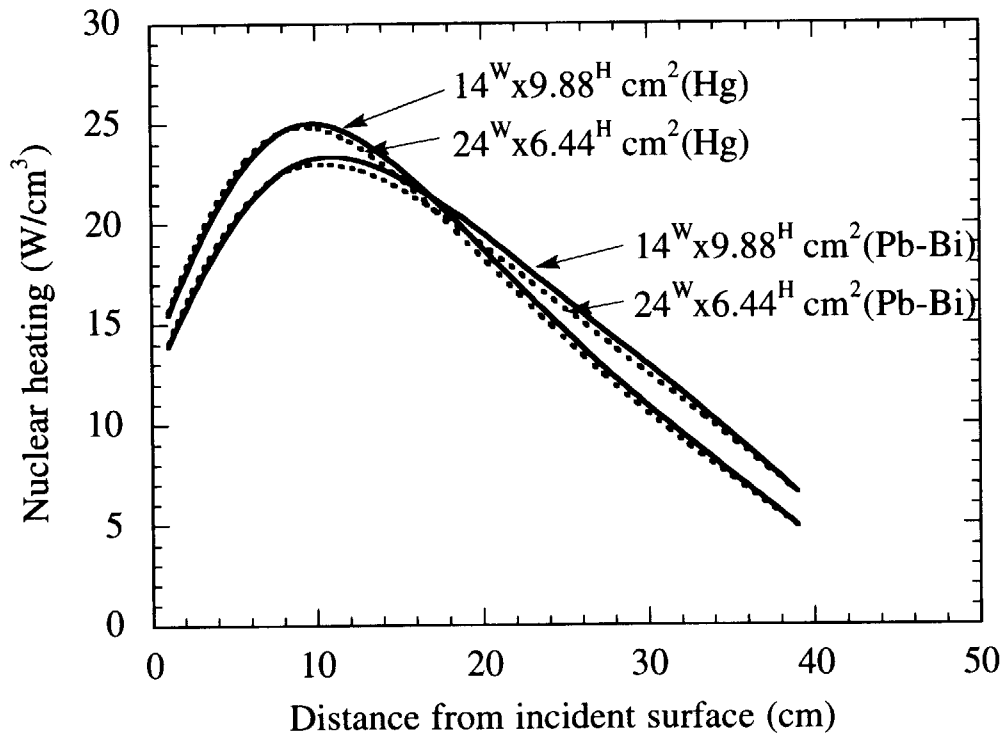


Fig. 19 Axial distribution of nuclear heating in a  $1 \text{ cm}^3 \text{ H}_2\text{O}$  sample at 2 cm from target surface faced to moderator for proton beam power of 5 MW

# 国際単位系 (SI) と換算表

表1 SI基本単位および補助単位

量	名称	記号
長さ	メートル	m
質量	キログラム	kg
時間	秒	s
電流	アンペア	A
熱力学温度	ケルビン	K
物質質量	モル	mol
光度	カンデラ	cd
平面角	ラジアン	rad
立体角	ステラジアン	sr

表3 固有の名称をもつSI組立単位

量	名称	記号	他のSI単位による表現
周波数	ヘルツ	Hz	s <sup>-1</sup>
力	ニュートン	N	m·kg/s <sup>2</sup>
圧力, 応力	パスカル	Pa	N/m <sup>2</sup>
エネルギー, 仕事, 熱量	ジュール	J	N·m
上率, 放射束	ワット	W	J/s
電気量, 電荷	クーロン	C	A·s
電位, 電圧, 起電力	ボルト	V	W/A
静電容量	ファラド	F	C/V
電気抵抗	オーム	Ω	V/A
コンダクタンス	ジーメン	S	A/V
磁束	ウェーバ	Wb	V·s
磁束密度	テスラ	T	Wb/m <sup>2</sup>
インダクタンス	ヘンリー	H	Wb/A
セルシウス温度	セルシウス度	°C	
光束	ルーメン	lm	cd·sr
照射度	ルクス	lx	lm/m <sup>2</sup>
放射能	ベクレル	Bq	s <sup>-1</sup>
吸収線量	グレイ	Gy	J/kg
線量当量	シーベルト	Sv	J/kg

表2 SIと併用される単位

名称	記号
分, 時, 日	min, h, d
度, 分, 秒	°, ', "
リットル	l, L
トン	t
電子ボルト	eV
原子質量単位	u

1 eV = 1.60218 × 10<sup>-19</sup> J  
 1 u = 1.66054 × 10<sup>-27</sup> kg

表4 SIと共に暫定的に維持される単位

名称	記号
オングストローム	Å
バーン	b
バル	bar
ガリ	Gal
キュリー	Ci
レントゲン	R
ラド	rad
レム	rem

1 Å = 0.1 nm = 10<sup>-10</sup> m  
 1 b = 100 fm<sup>2</sup> = 10<sup>-28</sup> m<sup>2</sup>  
 1 bar = 0.1 MPa = 10<sup>5</sup> Pa  
 1 Gal = 1 cm/s<sup>2</sup> = 10<sup>-2</sup> m/s<sup>2</sup>  
 1 Ci = 3.7 × 10<sup>10</sup> Bq  
 1 R = 2.58 × 10<sup>-4</sup> C/kg  
 1 rad = 1 cGy = 10<sup>-2</sup> Gy  
 1 rem = 1 cSv = 10<sup>-2</sup> Sv

表5 SI接頭語

倍数	接頭語	記号
10 <sup>18</sup>	エクサ	E
10 <sup>15</sup>	ペタ	P
10 <sup>12</sup>	テラ	T
10 <sup>9</sup>	ギガ	G
10 <sup>6</sup>	メガ	M
10 <sup>3</sup>	キロ	k
10 <sup>2</sup>	ヘクト	h
10 <sup>1</sup>	デカ	da
10 <sup>-1</sup>	デシ	d
10 <sup>-2</sup>	センチ	c
10 <sup>-3</sup>	ミリ	m
10 <sup>-6</sup>	マイクロ	μ
10 <sup>-9</sup>	ナノ	n
10 <sup>-12</sup>	ピコ	p
10 <sup>-15</sup>	フェムト	f
10 <sup>-18</sup>	アト	a

(注)

- 表1 5は「国際単位系」第5版, 国際度量衡局 1985年刊行による。ただし, 1 eV および 1 uの値はCODATAの1986年推奨値によった。
- 表4には海里, ノット, アール, ヘクタールも含まれているが日常の単位なのでここでは省略した。
- barは, JISでは流体の圧力を表わす場合に限り表2のカテゴリーに分類されている。
- EC閣僚理事会指令ではbar, barnおよび「血圧の単位」mmHgを表2のカテゴリーに入れている。

## 換 算 表

力	N (=10 <sup>5</sup> dyn)	kgf	lbf
	1	0.101972	0.224809
	9.80665	1	2.20462
	4.44822	0.453592	1

粘度 1 Pa·s (N·s/m<sup>2</sup>) = 10 P (ポアズ) (g/(cm·s))  
 動粘度 1 m<sup>2</sup>/s = 10<sup>4</sup> St (ストークス) (cm<sup>2</sup>/s)

圧	MPa (=10 bar)	kgf/cm <sup>2</sup>	atm	mmHg (Torr)	lbf/in <sup>2</sup> (psi)
	1	10.1972	9.86923	7.50062 × 10 <sup>3</sup>	145.038
力	0.0980665	1	0.967841	735.559	14.2233
	0.101325	1.03323	1	760	14.6959
	1.33322 × 10 <sup>-4</sup>	1.35951 × 10 <sup>-3</sup>	1.31579 × 10 <sup>-3</sup>	1	1.93368 × 10 <sup>-2</sup>
	6.89476 × 10 <sup>-3</sup>	7.03070 × 10 <sup>-2</sup>	6.80460 × 10 <sup>-2</sup>	51.7149	1

エネルギー・仕事・熱量	J (=10 <sup>7</sup> erg)	kgf·m	kW·h	cal (計量法)	Btu	ft·lbf	eV
	1	0.101972	2.77778 × 10 <sup>-7</sup>	0.238889	9.47813 × 10 <sup>-4</sup>	0.737562	6.24150 × 10 <sup>18</sup>
	9.80665	1	2.72407 × 10 <sup>-6</sup>	2.34270	9.29487 × 10 <sup>-3</sup>	7.23301	6.12082 × 10 <sup>19</sup>
	3.6 × 10 <sup>6</sup>	3.67098 × 10 <sup>5</sup>	1	8.59999 × 10 <sup>5</sup>	3412.13	2.65522 × 10 <sup>6</sup>	2.24694 × 10 <sup>25</sup>
	4.18605	0.426858	1.16279 × 10 <sup>-6</sup>	1	3.96759 × 10 <sup>-3</sup>	3.08747	2.61272 × 10 <sup>19</sup>
	1055.06	107.586	2.93072 × 10 <sup>-4</sup>	252.042	1	778.172	6.58515 × 10 <sup>21</sup>
	1.35582	0.138255	3.76616 × 10 <sup>-7</sup>	0.323890	1.28506 × 10 <sup>-3</sup>	1	8.46233 × 10 <sup>18</sup>
	1.60218 × 10 <sup>-19</sup>	1.63377 × 10 <sup>-20</sup>	4.45050 × 10 <sup>-26</sup>	3.82743 × 10 <sup>-20</sup>	1.51857 × 10 <sup>-22</sup>	1.18171 × 10 <sup>-19</sup>	1

1 cal = 4.18605 J (計量法)  
 = 4.184 J (熱化学)  
 = 4.1855 J (15 °C)  
 = 4.1868 J (国際蒸気表)  
 仕事率 1 PS (仏馬力)  
 = 75 kgf·m/s  
 = 735.499 W

放射能	Bq	Ci
	1	2.70270 × 10 <sup>-11</sup>
	3.7 × 10 <sup>10</sup>	1

吸収線量	Gy	rad
	1	100
	0.01	1

照射線量	C/kg	R
	1	3876
	2.58 × 10 <sup>-4</sup>	1

線量当量	Sv	rem
	1	100
	0.01	1

